ACS APPLIED MATERIALS & INTERFACES
Research Article
www.acsami.org

Solution-Based Synthesis of Crystalline Silicon from Liquid Silane through Laser and Chemical Annealing

Ganjigunte R. S. Iyer,[†] Erik K. Hobbie,*[,†] Srinivasan Guruvenket,[‡] Justin M. Hoey,[‡] Kenneth J. Anderson,[‡] John Lovaasen,[‡] Cody Gette,[‡] Douglas L. Schulz,[‡] Orven F. Swenson,[‡] Arumugasamy Elangovan,[‡] and P. Boudjouk[‡]

[†]Department of Physics and Department of Coatings and Polymeric Materials, and [‡]Center for Nanoscale Science and Engineering, North Dakota State University, Fargo, North Dakota 58102, United States

Supporting Information

ABSTRACT: We report a solution process for the synthesis of crystalline silicon from the liquid silane precursor cyclohexasilane (Si_6H_{12}). Polysilane films were crystallized through thermal and laser annealing, with plasma hydrogenation at atmospheric pressure generating further structural changes in the films. The evolution from amorphous to microcrystalline is characterized using scanning electron microscopy (SEM), atomic force microscopy (AFM), Raman spectroscopy and impedance spectroscopy. A four-decade enhancement in the electrical conductivity is attributed to a disorder−order transition in a bonded Si network. Our results demonstrate a potentially attractive approach that employs a solution process coupled with ambient postprocessing to produce crystalline silicon thin films.

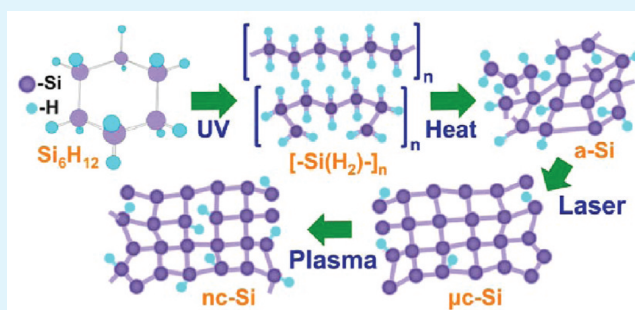

KEYWORDS: *silicon, liquid silane, laser crystallization, plasma annealing*

INTRODUCTION

Silicon (Si) dominates the semiconductor electronics industry for a number of applications, ranging from microelectronic devices and thin film transistors to imaging sensors and solar cells.[1] The ability of Si to form either *p* or *n*-type materials through preferential doping is critical to most of these applications. Although a significant effort has been directed at synthesizing new semiconductor materials, silicon still accounts for the majority of material used in the industry, mostly in the form of single-crystal wafer Si (c-Si). Alternatively, thin films of amorphous Si (a-Si), microcrystalline Si (μc-Si) and nanocrystalline Si (nc-Si), whose synthesis has been popularized primarily through vacuum-based techniques such as plasma-enhanced chemical vapor deposition (PECVD), have emerged as promising potential replacements for c-Si in some applications.

Silicon analogues of alkane hydrocarbons include monosilane (SiH_4), disilane (Si_2H_6), trisilane (Si_3H_8) and tetrasilane (Si_4H_{10}), of which SiH_4 gas and/or SiH_4/H_2 gas mixtures are most commonly used in PECVD. However, the translation of these precursor systems to high-throughput roll-to-roll manufacturing is hampered by challenges associated with handling the highly pyrophoric silane gases and the batch nature of CVD, which puts limits on substrate size and throughput scalability. As an alternative to conventional vacuum processes, a considerable amount of research has been directed at solution-based methods, such as spin coating, spray coating and electro-spinning.[2−11] These "wet" processes have the potential to become viable, cost-effective methods for generating patterned or even large-area electronic thin films, and the use of a liquid precursor offers the attractive possibility of developing devices in a manner analogous to inkjet printing. In this view, a liquid-based approach is particularly appealing for applications that demand the high-throughput production of repetitive localized features, such as lines and dots, with varied or inhomogeneous doping.

Electronic grade inorganic semiconductor materials, such as ZnO and the metal chalcogenides,[8−11] have recently been realized through solution processing, but relatively little progress has been reported in this regard for silicon, despite significant effort. Cyclopentasilane (CPS, Si_5H_{10}) is a liquid silane precursor commonly used in both vacuum and solution based deposition.[5] Hengge et al.[12−16] demonstrated that ring-opening polymerization of the cyclic silanes upon irradiation with ultraviolet (UV) light leads to a hydrogen-rich linear Si chain, and Shimoda et al.[5] have successfully obtained polycrystalline silicon films through the UV ring-opening polymerization of CPS, which forms a white solid mixture of hydrogenated polysilanes that can be partially dissolved in organic solvents but requires filtration prior to spin coating.

Received: February 24, 2012
Accepted: April 30, 2012
Published: April 30, 2012

 © 2012 American Chemical Society

Although this represents a path forward in liquid-based silicon processing, it still involves multiple steps, marginal solubility, and is plagued by poor substrate wetting due to the excess CPS monomer required for dispersion.

Among the various cyclic silanes, cyclohexasilane (CHS, Si_6H_{12}) is particularly interesting because it maintains a low vapor pressure and is stable in ambient light. Like CPS, CHS can also be used for the solution-based synthesis of functional Si thin films.[17−20] A synthetic route to liquid CHS was previously reported, where the reaction of $HSiCl_3$ with a polyamine gives a salt containing the $[Si_6Cl_{14}]^{2-}$ dianion, which is readily reduced to Si_6H_{12}.[17−19] The silane undergoes a ring-opening polymerization when exposed to heat or UV light, with thermal annealing transforming the polyhydrosilane to thin-film silicon. In this context, drawing motivation from the current interest in nonvacuum, solution-based approaches, we report a process for the synthesis of micro- and nanocrystalline Si from liquid CHS in a platform that is readily applicable to "printing" applications. Here, we focus specifically on how the structural and electronic properties of liquid processed Si films evolve with thermal annealing, laser crystallization and hydrogen-plasma treatment.

■ EXPERIMENTAL SECTION

Purified CHS was synthesized in-house and the organic solvent cyclooctane (≥99% purity, Sigma Aldrich) was sparged with N_2 prior to use. Spin coating and initial heat treatment were carried out in dry nitrogen using a glovebox (<1 ppm O_2) to avoid oxidation. Figure 1 shows a schematic of the process. The precursor ink (CHS) is spin-coated (500 rpm for 60 s, ramping up to 2000 rpm for 30 s) on a substrate (quartz or wafer Si) at room temperature under simultaneous UV irradiation from a 500 W HgXe lamp to initiate ring-opening polymerization into polysilane, denoted $[-Si(H_2)-]_n$. The thin film thus formed is then annealed at 400 °C for 1 h on a hot plate to transform it to amorphous silicon through the elimination of excess hydrogen. The film is then subjected to tube furnace annealing at 550 °C for 1 h in a nitrogen atmosphere to induce further desorption of hydrogen, and then subjected to laser irradiation (355 nm, 375 mW pulsed laser, rastered at 25 mm/s) in ambient to produce μc-Si. The amorphous silicon films are referred to as ASF, the thermally treated Si films as TTSF, and the laser-treated Si films as LTSF.

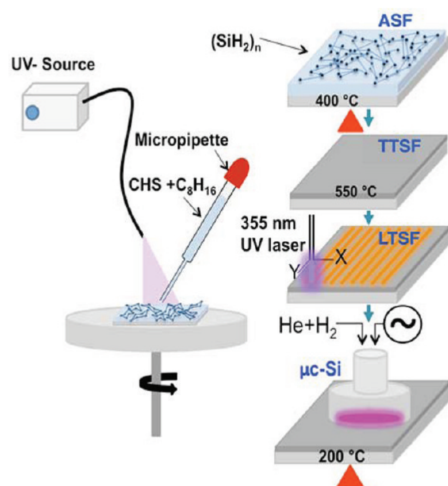

Figure 1. Schematic of the solution-based synthesis of microcrystalline silicon (μc-Si) thin films.

In the final step, the LTSF samples are hydrogen-plasma treated to study chemical annealing effects induced by H insertion into the Si matrix. Plasma treatment was performed in a glovebox with a Surfx Atomflo 250D atmospheric pressure plasma (APP) source operated at 13.56 MHz and 80 W with He (plasma gas) and H_2 (reactive gas) flowing at 30 and 0.15 L/min, respectively. Six LTSF samples were treated for times ranging from 5 to 30 min in steps of 5 min, with the substrate maintained at 200 °C. APP is a nonvacuum process performed at ambient pressure and temperature in an atmosphere of N_2. Plasma treated LTSF samples with treatment times between 0 and 30 min are referred to as H-0, H-5, H-10, H-15, H-20, H-25, and H-30, respectively. After the thermal, laser, or plasma treatments, aluminum contacts (250 nm thickness) were sputtered through a shadow mask (0.185 mm width and 2.625 mm length) to facilitate conductivity measurements of the films. Deposition of electrodes either before or after plasma treatment had no influence on the results.

Structural changes in the Si films were evaluated with microscopy and spectroscopy. Morphological changes were observed with scanning electron microscopy (SEM) and atomic force microscopy (AFM). For SEM, the sample was attached to an aluminum mount using carbon double-sided tape and imaged using a JEOL JSM-7600F field-emission scanning electron microscope operating at either 2.00 kV or 5.00 kV in secondary electron imaging (SEI) mode. Grounded copper tape connected to the films with silver epoxy was used to mitigate sample-charging effects. The local topography and grain size were measured with AFM in tapping mode using gold-coated n-type Si tips (10 nm radius, 3.0 N/m nominal force constant and 60 kHz nominal resonant frequency) on a Veeco Nanoscope III instrument. Microstructural changes were also studied by Raman spectroscopy using a HORIBA Jobin Yvon LabRAM ARAMIS confocal imaging system with a 532 nm Nd:YAG laser and 100x objective. An average of eight spots were chosen for each sample. Film conductivity was measured on an Agilent B1500A semiconductor analyzer both before and after plasma treatment. Conductivity measurements were performed in air and in the dark inside a grounded metal shell. Film thickness was measured using a VASE spectroscopic ellipsometer (J. A. Woollam) operated at three angles of incidence (60, 67, and 74°) over the range 260−760 nm in steps of 10 nm, and the average film thickness (60 nm) was determined using WVASE software.

■ RESULTS AND DISCUSSION

Chemical and structural changes that occur in the films during processing can have a profound impact on applications. Here, we focus on changes associated with the evolution from liquid to solid (both amorphous and crystalline) and the effect of hydrogen plasma post-treatment on the microcrystalline films. Figure 2 shows the evolution of the ASF morphology in response to thermal and laser treatments. The ASF (Figure 2a)

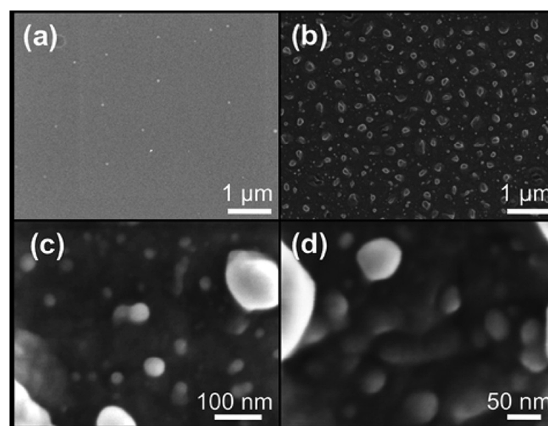

Figure 2. SEM micrographs of an (a) ASF, (b) TTSF, (c) LTSF, and (d) LTSF at higher magnification.

dx.doi.org/10.1021/am300334p | ACS Appl. Mater. Interfaces 2012, 4, 2680−2685

appears smooth and uniform, while the TTSF (Figure 2b) is broken down into clusters. Upon laser treatment, the films further fragment into a broad distribution of cluster sizes (Figure 2c,d). Surface topography measurements with AFM reveal the effect of initial heat treatment on the average surface roughness, R_a. The ASFs were smooth ($R_a \approx 5$ nm) with an average grain-size of 1.5 nm (Figure 3a). Interestingly, while the

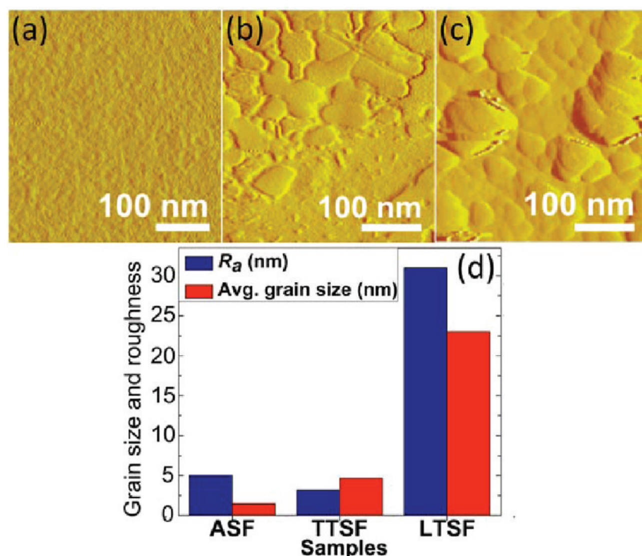

Figure 3. AFM (amplitude) images (1 μm^2) of (a) ASF, (b) TTSF, (c) LTSF, and (d) the average roughness and grain size of the processed samples. Uncertainty in the roughness and grain size is 5%.

R_a of the TTSFs decreased by a few nanometers, the average grain size increased from 1.5 to 5 nm. The LTSFs showed enhanced crystallization, with a broad distribution of cluster sizes (Figure 3c). The R_a of the laser treated films also increased to ~30 nm, which might be attributed to rapid solidification. Figure 3d summarizes the evolution of R_a and the average crystallite size. In classic PECVD growth, vapor molecules nucleate on a surface to form a thin film with nanoscale smoothness,[21,22] whereas solution processes have been reported to produce films with significantly higher roughness.

Figure 4a shows an overlay of Raman spectra for ASF, TTSF, and LTSF samples, which show an evolution from a broad peak of predominantly amorphous phase to a sharp peak indicative of crystallinity. For clarity, the baseline has been vertically shifted by a constant for each spectrum. The a-Si peak shows a broad transverse-optical (TO) phonon mode at ~480 cm^{-1} (black), while the dominant peak at 515 cm^{-1} in the LTSF is attributed to the TO mode of Si–Si vibrations, indicating a transition from a-Si to crystalline Si (the peak is near 521 cm^{-1} for a pure, unstrained crystalline phase).[23,24] On the basis of the deconvoluted spectrum of a laser treated film (Figure 4b), three different phases can be identified; (i) a sharp TO mode due to microcrystalline Si near 515 cm^{-1}, (ii) an intermediate peak at 509 cm^{-1} due to defects and grain boundaries, and (iii) a broad peak at 484 cm^{-1} from amorphous silicon.[23−27] The crystalline volume fraction (X_c) follows from the deconvoluted spectra as[23−27]

$$X_c = \frac{I_c + I_m}{I_c + I_m + \beta I_a} \quad (1)$$

where I_c, I_m, and I_a are the integrated intensities of the crystalline, intermediate, and amorphous peaks, respectively, and β is the ratio of the integrated Raman cross-section of the amorphous phase to that of the crystalline phase. In the nanocrystal range, β is typically close to unity.[23−27] Accordingly, the crystalline fraction of the laser-treated films is approaching 95%.

Rapid solidification can induce stress or strain in the film. Here, the crystalline TO mode in the LTSF is observed at lower frequencies than the usual crystalline peak (i.e., at 515 cm^{-1} as opposed to 521 cm^{-1}), indicative of stress in the film. In the case of a strained Si layer with an in-plane stress σ, the anticipated correlation is[28] $\sigma = -0.2\Delta\omega$, where $\Delta\omega$ (measured in cm^{-1}) is the frequency shift in the TO Raman signal from 521 cm^{-1} and σ (measured in GPa) is the stress. Compressive stress ($\sigma < 0$) results in an upward shift, while tensile stress ($\sigma > 0$) results in a downward shift. These observations suggest that the LTSF is under tensile stress, which is detrimental to film performance.[29,30] To clarify the impact of microstructural change on the electronic transport properties of the films, we performed conductivity measurements on the ASF, TTSF and LTSF samples. The resistance of the a-Si films decreased by 3 orders of magnitude in response to laser treatment (30×10^{12} Ω to 1×10^{9} Ω). Through rapid annealing, the laser treatment promotes the amorphous-to-crystalline transition, but with residual tensile stress. Isochronal annealing and hydrogen plasma treatment (chemical annealing) are most commonly

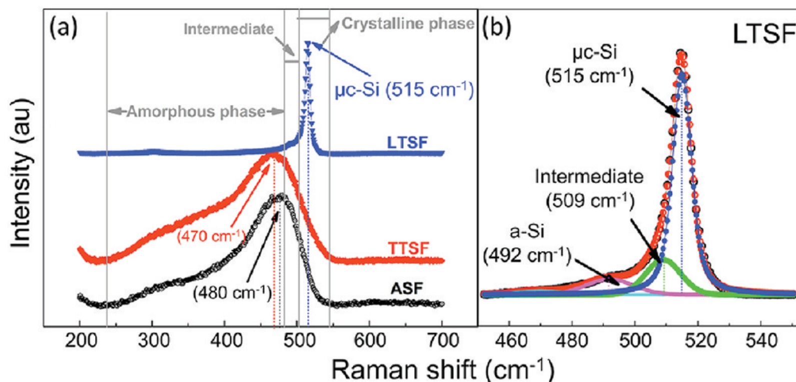

Figure 4. (a) Overlay of Raman spectra for the ASF, TTSF and LTSF, where the baseline of each spectrum has been vertically shifted by a constant for clarity. (b) A deconvolution showing the underlying peak structure for an LTSF sample.

dx.doi.org/10.1021/am300334p | ACS Appl. Mater. Interfaces 2012, 4, 2680−2685

used to remove this stress,[31] and here we use He + H_2 plasma treatment, as detailed below.

Hydrogenated silicon thin films synthesized through PECVD and PVD have been studied extensively, and it is well established that hydrogen plays a crucial role in controlling the structure through a-Si:H and μc-Si:H. Generally, disordered or amorphous films contain predominantly unsaturated Si−Si bonds, with an increased density of localized defects. To passivate these, it is necessary to introduce atoms of a smaller diameter, and hydrogen is most commonly used in this regard. The introduction of hydrogen induces crystallization by facilitating hydrogen insertion into dangling bonds or defects.[32] There have been several reports of hydrogen-mediated crystallization in silicon films, either by hydrogen dilution during growth or as a post-treatment process.[22,32] The influence of hydrogen plasma treatment on the morphology, microstructure, optical and electronic properties of these materials is potentially important.

Time-dependent H-plasma treatment of the LTSFs was thus carried out for 5−30 min (in 5 min increments) and subsequent changes in morphology, topography, and conductivity were measured. Figure 5 shows SEM images of the LTSFs subjected to plasma treatment for various time intervals. At increased treatment times, the films are further crystallized, but the clusters are broken down into smaller crystallites (Figure 5b). Figure 6 illustrates the changes in surface topography and roughness after plasma treatment of the same samples, and the results are consistent with the morphological changes suggested by SEM. The untreated LTSF films (H-0, Figure 6a) consist of mostly crystallites or scattered clusters of 20−30 nm grains, but these features are significantly modified by the plasma treatment.

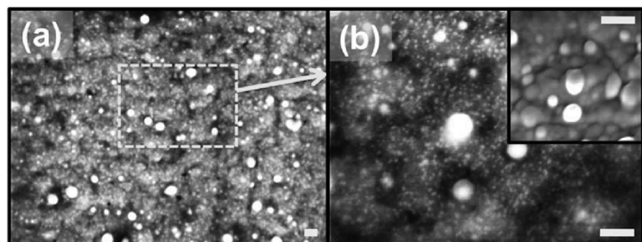

Figure 5. (a) SEM micrograph of a film H-plasma treated for 20 min (H-20), where (b) is a magnified image of a. The inset to b is a magnified image of an H-30 film. The scale bar in each image is 100 nm.

Plasma treatment for 20 min (H-20, Figure 6b) changes the average roughness from 30 to 18 nm, whereas the grain size decreases from 23 to 15 nm. Plasma treatment for longer times (H-30, Figure 6c) breaks the clusters down further (~7 nm grains), whereas the average roughness further decreases to <10 nm. Figure 7a is an overlay of Raman data for the Si films at different treatment times, where the inset presents a summary of how the peak position evolves with plasma treatment. Figure 7b shows the deconvolution of a Raman spectrum from an LTSF sample treated for 20 min. Figure 7c shows the deconvolution of the same sample treated for 30 min, where the microstructure has been further transformed. From the overlay in Figure 7a, the TO Raman peak shits up to ~517 cm^{-1} during early treatment, which is consistent with what has been reported for H-plasma treated a-Si:H films grown with PECVD.[21,25,33] At longer processing times, however, there is a downward shift of the TO peak accompanied by a small intermediate peak, consistent with an "order−disorder" transformation (ODT).

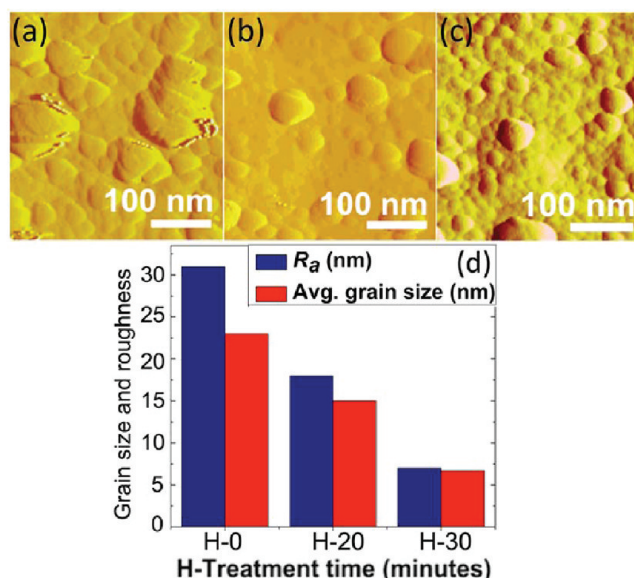

Figure 6. Topographical (amplitude) images of (a) the reference LTSF (H-0), (b) H-20, (c) H-30, and (d) the average roughness and average grain size. The scale bar in each image is 100 nm, and the uncertainty in the roughness and grain size is 5%.

For shorter treatment times, small concentrations of H get inserted into strained Si−Si bonds, passivating defects and leading to increased crystallization. For longer treatment times, however, the increased concentration of H may actually induce defects. These spectroscopic observations are in qualitative agreement with the morphological changes revealed by SEM and AFM, and the reported changes are further supported by Fourier transform infrared spectroscopy (FTIR), as detailed in the Supporting Information. The changes occurring at longer treatment times (beyond 20 min) are too subtle, however, to be easily detected in the time evolution of the crystalline volume fraction deduced from the integrated Raman intensities, as detailed in the Supporting Information.

Smooth, stress-free films are typically required for device fabrication. Reports based on vacuum deposition suggest that the attachment of impinging radicals and surface mobility can both impact surface roughness.[34,35] A substantial decrease in surface roughness and grain size with increased H-plasma treatment can be attributed to the diffusion-assisted mass transport and surface migration of Si atoms.[36] Surface diffusion and grain boundary diffusion are the two main pathways to surface modification.[22,36] Sriram et al. used molecular level simulations, for example, to study H diffusion in a-Si:H by successive hopping through Si−Si bonds, thereby mediating crystallization.[37,38]

Figure 8 shows the effect of H-plasma treatment on the conductivity of the laser treated films. The conductivity is initially enhanced up to a maximum near H-20, but then starts to decrease with longer treatment times. The curve in Figure 8 is a fit to the generic power-law expression $\sigma = \sigma_{\pm}|t - t|^{-\alpha}$ with $\alpha \approx 3$ and a critical treatment time (t_c) of 19 min. As anticipated, the evolution of the conductivity follows the change in microstructure described above, although the measured conductivity is much higher than that of intrinsic c-Si. Secondary ion mass spectrometry (SIMS) revealed ≤1 ppm

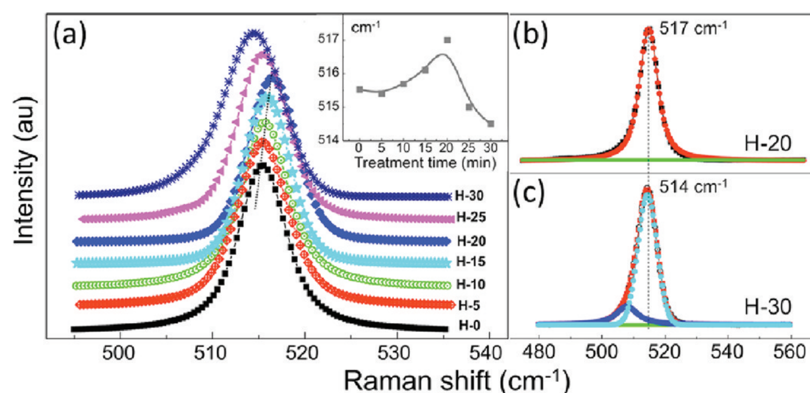

Figure 7. (a) Overlay of Raman spectra for the H-plasma-treated Si films after various treatment times. The baseline of each spectrum has been vertically shifted by a constant for clarity. The inset shows the peak position as a function of plasma treatment time. Deconvoluted spectra of (b) H-20 and (c) H-30.

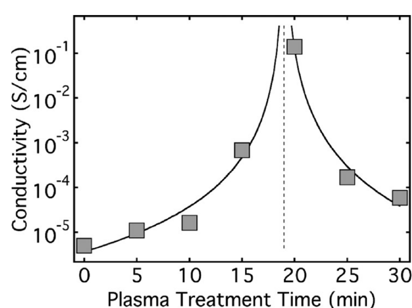

Figure 8. Conductivity of the crystalline Si films as a function of H-plasma treatment time. Error bars are the size of the data markers.

concentrations of Al, Li, and Ti in the ASF samples, where these impurities are a result of the CHS synthesis scheme and were specifically targeted to test the effectiveness of the purification method. It is well established that such impurities can enhance the conductivity through doping and other effects. Because the inks will ultimately be intentionally doped, it is not yet clear how important such impurity levels will be, and this question is the subject of ongoing investigations. The plasma-treated samples were tested for stability over a period of 2 months with no signs of deterioration from exposure to air or sunlight.

■ CONCLUSIONS

We report a process for the synthesis of crystalline silicon from the liquid silane precursor CHS. Spin-coated polysilane thin films are subsequently crystallized through a combination of thermal and laser annealing, and ambient hydrogen plasma treatment is used to further enhance the structural and electronic properties of the films. Layer-by-layer growth through successive chemical reactions may not be possible with solution processed Si films, but our results demonstrate that the structure can still be engineered through successive processes. Undesirable effects such as stress or defects are typically addressed through thermal treatment or low-energy ion bombardment, but here we use a relatively unexplored nonvacuum APP method. Atomically smooth amorphous silicon films have been achieved with conventional methods such as PVD, CVD and PECVD, mostly through hydrogen dilution during deposition. In our case, the solution processed amorphous Si films exhibit grain sizes on the order of 2 nm. The key to obtaining a smooth initial film is uniform photo polymerization of the silane ink with UV light during spin-coating, which limits any dewetting of the film.

For amorphous films with dangling or strained Si−Si bonds, increased thermal energy results in the rearrangement of Si−H. Laser irradiation further enables the out-diffusion of hydrogen, thereby promoting crystallization. The increase in average roughness indicates clustering due to rapid annealing and the subsequent agglomeration of clusters. The emergence of a dominant TO Raman mode at 517 cm^{-1} (downshifted with respect to that of single-crystal Si at 521 cm^{-1}) is indicative of small residual tensile stress in the film. For short H treatment times, increased crystallinity can be attributed to both H insertion into strained Si−Si bonds and H diffusion through grain boundaries. For longer H-treatment times, however, the crystallinity may be somewhat reduced, while the increase in concentration of H and Si−H reduces the number of possible conduction pathways. A disorder−order−disorder transition with a four-decade increase in conductivity is clearly evident in the electronic properties of the films, and this transition is mirrored by changes in microstructure. Overall, the results we present here are encouraging as a potential solution-based process for generating crystalline Si from a liquid silane precursor.

■ ASSOCIATED CONTENT

Supporting Information

FTIR measurements and a discussion of the crystalline volume fraction as a function of plasma treatment time. This material is available free of charge via the Internet at http://pubs.acs.org.

■ AUTHOR INFORMATION

Corresponding Author

*E-mail: erik.hobbie@ndsu.edu.

Notes

The authors declare no competing financial interest.

■ ACKNOWLEDGMENTS

This research has been sponsored by the Department of Energy through DE-FG36-08GO88160. The views and conclusions contained herein are those of the authors and should not be interpreted as necessarily representing the official policies or endorsements, either expressed or implied, of the Department of Energy or the U.S. Government.

REFERENCES

(1) Zimmermann, H. K. *Integrated Silicon Optoelectronics*; Springer: Berlin, 2010.
(2) Heath, J. R. *Science* **1992**, *258*, 1131−1133.
(3) Sirringhaus, H. *Adv. Mater.* **2005**, *17*, 2411−2425.
(4) Zaumseil, J.; Sirringhaus, H. *Chem. Rev.* **2007**, *107*, 1296−1323.
(5) Shimoda, T.; Matsuki, Y.; Furusawa, M.; Aoki, T.; Yudasaka, I.; Tanaka, H.; Iwasawa, H.; Wang, D.; Miyasaka, M.; Takeuchi, Y. *Nature* **2006**, *440*, 783−786.
(6) Kim, S.; Han, T. H.; Jung, H. C.; Oh, Y. S.; Pu, L.; Lee, P. C.; Nam, J. D. *J. Mater. Chem.* **2011**, *21*, 3025−3029.
(7) Kim, S.; Lee, C. Y.; Jin, M. H. C. *Sol. Energy Mater. Sol. Cells* **2012**, *100*, 61−64.
(8) Todorov, T. K.; Reuter, K. B.; Mitzi, D. B. *Adv. Mater.* **2010**, *22*, 156−159.
(9) Hoffmann, R. C.; Dilfer, S.; Issanin, A.; Scheinder, J. J. *Phys. Status Solidi A* **2010**, *207*, 1590−1595.
(10) Mitzi, D. B.; Kosbar, L. L.; Murray, C. E.; Copel, M.; Afzali, A. *Nature* **2004**, *428*, 299−303.
(11) Mitzi, D. B. *Solution Processing of Inorganic Materials*; John Wiley & Sons: New York, 2009.
(12) Hengge, E.; Stüger, H. *PATAI'S Chemistry of Functional Groups*; John Wiley & Sons: New York, 2009.
(13) Hengge, E.; Marketz, H. *Monatsh. Chem.* **1970**, *101*, 528−534.
(14) Hengge, E.; Bauer, G. *Angew. Chem., Int. Ed.* **1973**, *12*, 316−316.
(15) Hengge, E.; Janoschek, R. *Chem. Rev.* **1995**, *95*, 1495−1526.
(16) Hengge, E.; Bauer, G. *Monatsh. Chem.* **1975**, *106*, 503−512.
(17) Boudjouk, P.; Kim, B. K.; Remington, M. P.; Chauhan, B. United States Patent 5 942 637, August 24, 1999.
(18) Choi, S. B.; Kim, B. K.; Boudjouk, P.; Grier, D. G. *J. Am. Chem. Soc.* **2001**, *123*, 8117−8118.
(19) Elangovan, A.; Anderson, K.; Schulz, D.; Boudjouk, P. WIPO Patent WO2011094191, Jan 25, 2011.
(20) Han, S.; Dai, X.; Loy, P.; Lovaasen, J.; Huether, L.; Hoey, J. M.; Wagner, A.; Sandstrom, J.; Bunzow, D.; Swenson, O. F.; Akhatov, I. S.; Schulz, D. L. *J. Non-Cryst. Solids* **2008**, *354*, 2623−2626.
(21) Jin, J.; Yuan, Z.; Huang, L.; Chen, S.; Shi, W.; Cao, Z.; Lou, Q. *Appl. Surf. Sci.* **2010**, *256*, 3453−3458.
(22) Dutta, P.; Paul, S.; Galipeau, D.; Bommisetty, V. *Thin Solid Films* **2010**, *518*, 6811−6817.
(23) Song, D.; Cho, E. C.; Conibeer, G.; Flynn, C.; Huang, Y.; Green, M. A. *Sol. Energy Mater. Sol. Cells* **2008**, *92*, 474−481.
(24) Sumita, M.; Das, C.; Ray, S. *J. Phys. D: Appl. Phys.* **2004**, *37*, 1736−1741.
(25) Cheng, Q.; Xu, S.; Ostrikov, K. *J. Mater. Chem.* **2009**, *19*, 5134−5140.
(26) Liu, S.; Zeng, X.; Peng, W.; Xiao, H.; Yao, W.; Xie, X.; Wang, C.; Wang, Z. *J. Non-Cryst. Solids* **2011**, *357*, 121−125.
(27) Han, D.; Wang, K.; Owens, J. M.; Gedvilas, L.; Nelson, B.; Habuchi, H.; Tanaka, M. *J. Appl. Phys.* **2003**, *93*, 3776−3783.
(28) Wolf, I. D. *Semicond. Sci. Technol.* **1996**, *11*, 139−154.
(29) Bonera, E.; Fanciulli, M.; Mariani, M. *Appl. Phys. Lett.* **2005**, *87*, 111913−111915.
(30) Lengsfeld, P.; Nickel, N. H.; Genzel, C.; Fuhs, W. *J. Appl. Phys.* **2002**, *91*, 9128−9135.
(31) Ohmi, H.; Kakiuchi, H.; Nishijima, K.; Watanabe, H.; Yasutake, K. *Jpn. J. Appl. Phys.* **2006**, *45*, 8488−8493.
(32) Sriraman, S.; Agarwal, S.; Aydil, E. S.; Maroudas, D. *Nature* **2002**, *418*, 62−65.
(33) Trung, T. Q.; Jiri, S.; Stuchlikova, H.; Binh, L. K.; Dinh, N. N.; Khuong, H. K.; Quynh, P. T. N.; Nga, N. T. H. *J. Phys. (Paris)* **2009**, *187*, 0120351−0120356.
(34) Ramalingam, S.; Sriraman, S.; Aydil, E. S.; Maroudas, D. *Appl. Phys. Lett.* **2001**, *78*, 2685−2687.
(35) Doughty, D. A.; Doyle, J. R.; Lin, G. H.; Gallagher, A. *J. Appl. Phys.* **1990**, *67*, 6220−6228.
(36) Ohring, M. *Materials Science of Thin Fims*; Elsevier: Singapore, 2006.
(37) Sriraman, S.; Aydil, E. S.; Maroudas, D. *J. Appl. Phys.* **2004**, *95*, 1792−1805.
(38) Sriraman, S.; Valipa, M. S.; Aydil, E. S.; Maroudas, D. *J. Appl. Phys.* **2006**, *100*, 053514−053524.